ARMA 19–1951

Numerical modelling of the influence of in-situ stress, rock strength and hole-profile geometry on the stability of Radial Water Jet Drill (RJD) boreholes

Latham[1], J-P., Farsi[1], A., Xiang[1], J., Clark[1], E. and Bakker[2] R.R.

1. Department of Earth Science and Engineering, Imperial College London, UK

2. Faculty of Civil Engineering and Geoscience, Technical University Delft, The Netherlands

ABSTRACT: Radial water jet drilling (RJD) is a method of enhancing heat recovery by accessing and connecting to high permeable zones within geothermal reservoirs. The wall rock geometry behind an advancing water jet borehole under in-situ conditions is largely unknown. Water jet drilling tests were performed on 300 mm cubical blocks of weak porous sandstone under true-triaxial boundary stress conditions at the Delft Technical University (DTU) rock mechanics laboratory. Some of these tests showed distinct breakout features depending on the applied stress field. Geometries of resulting boreholes are recovered using X-Ray CT scans, and are analysed using segmentation software (Avizo). The code Solidity, using a combined finite-discrete element method with a cohesive zone fracture model, simulates stress take-up and wall shearing giving breakouts comparable to the experiments. The results lead to the suggestion that criteria based on Kirsch solutions would be suitable to provide general guidance on in-situ stress and rock strength conditions free of breakouts. FEMDEM models appear well-suited to examine geometries and dimensions that can be sustained by given strengths under deeper in-situ conditions. Wall-rock failure and a process of jet-hole enlargement together with the potential benefits of greater heat recovery arising from larger holes is also briefly discussed.

1. INTRODUCTION

Radial Water-jet Drilling (RJD) uses the power of a focused jet of fluids, applied to a rock through a coil inserted in an existing well. The aim of developing this technology is to provide a cost effective alternative to hydraulic fracture stimulation, as a means to increase permeability and therefore heat flow for exploitation in geothermal energy production. Considerable international effort is therefore turning to the prediction of a rock type's 'jettability' as a function of (a) potentially controllable parameters e.g. jet nozzle design and head pressure for operating conditions, and (b) the uncontrollable rock properties and in-situ stress conditions in a reservoir. Laboratory testing and numerical methods are being applied to investigate factors contributing to rock jetting performance and rates of penetration as part of a wider scoped European H2020 project 'Novel Productivity Enhancement Concept for a Sustainable Utilization of a Geothermal Resource' (SURE) (see companion papers, this conference).

Jet drilling nozzle geometry and related technologies are undergoing innovative design modifications in search of a means to jet into deeper and harder rock. Currently, initiation and penetration of the jet at viable speeds remains a challenge for harder rocks and in down hole field conditions e.g. from 400 – 4000 m depth. Meanwhile, common RJD practice in sedimentary O&G reservoirs employs static and rotating nozzles which have forward and backward facing orifices to create both rock fabric damage in front and a means of propulsion behind the advancing head (Fig. 1). The prediction of field performance of jetting and the resulting hole geometries has been largely derived from laboratory tests on unconfined rock. Such geometries vary from back-thruster wash-out dominated star-shapes in soft limestones, conical profiles indicative of stop-start progression, to quite smooth cylindrical forms, depending on types of nozzle and rock type resistance.

The geometric form and dimensions of the jetted hole wall-rock as a conduit for hot fluid migration is of paramount importance to understanding enhancement of heat recovery. So too is the long-term stability of the lateral hole during service in a geothermal reservoir. Once jetted, the possible losses of fluid flow performance over time are considered to be mainly due to a combination of: (i) fines migration clogging, more common in reservoirs with argillite rock types and a

cited problem in Klaipeda, (Brehme et al., 2018) (ii) creep, e.g. thermally assisted creep leading to aperture reduction over time, (iii) geochemical precipitation (scale) causing aperture reduction and (iv) structural effects due to wall damage, breakouts, fragmentation, and possible blockages and clogging. The latter wall rock breakage, according to 3D FEM analysis considering circular tunnel advance, develops to its maximum at around two diameters behind the advancing hole (Eberhard 2001). At this distance and further behind the advancing front, wall differential stresses are fully amplified to their 2D plane strain state. Increased breakout features will occur the higher the ratios of wall rock tangential stress to UCS.

While considerable effort in the SURE project addresses 'jettability' and the factors governing rates of jet penetration under field conditions of in-situ stress and pore pressure, this paper focuses on the stability of the lateral in terms of the ultimate strength of the wall rock. Rather than considering time-dependent processes affecting long-term stability, it examines how rock deformation accommodates the changes in the triaxial stress state occurring at the time of the RJD excavation process, through failure and progressive fracturing.

Figure 1. RJD holes and nozzles: Left to right (top): principal of forward and backward thrusters in static nozzle, star-shaped profiles in soft limestone with unconfined rock and static nozzle. Left to right (bottom): conical stop-start geometries formed at head of rotating nozzle; detail of Beetle, BT 18 mm rotating nozzle available from "StoneAge" used in true-triaxial laboratory tests performed at TUDelft.

Solutions to the Kirsch Equations (Kirsch 1898) provide the starting point for a rich literature that predicts a rock's response to the excavation of cylindrical holes. However, whereas in tunnels and well-bores, the cross-sections imposed are highly prescribed, the shape immediately after jetting excavation is very uncertain and may differ greatly from cylindrical e.g. due to back-thruster jet action. Furthermore, many depths and in-situ stress conditions envisaged for RJD geothermal energy exploitation exceed failure conditions under which 'breakout' wall failure processes are predicted to occur and RJD laterals cannot be controlled by raised internal pressure e.g. through mud or water pressures within the

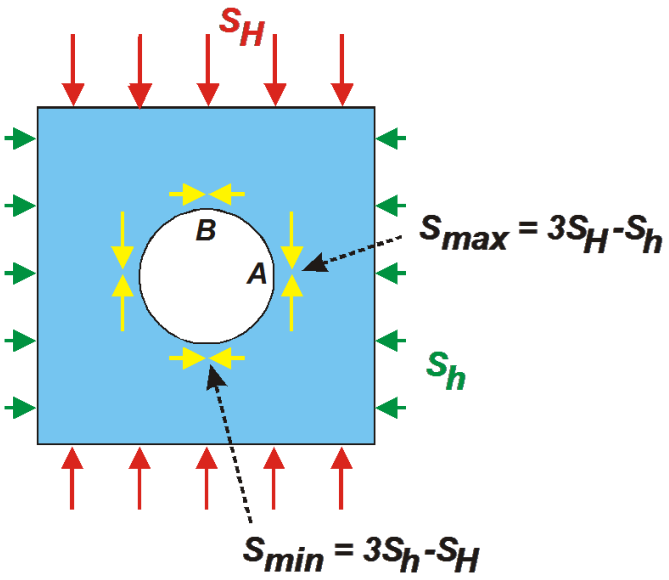

Figure 2. Kirsch solution for tangential stresses around wall of a vertical borehole.

hole. Methods to determine stability of circular tunnels, to plan well drilling with mud weight control of borehole breakouts and to measure in-situ stress using 'breakouts' apply simple criteria for the threshold of failure around circular openings. These criteria for strength to resist the wall-rock's tangential stress given by the Kirsch solution are based on fracture mechanics and/or strength of materials theory. When the maximum tangential compressive stress, σ_θ (= $3\sigma_{max} - \sigma_{min}$) generated in the wall of a cylindrical hole with far field maximum (σ_{max}) and minimum (σ_{min}) stresses across the hole, is greater than the rock's uniaxial compressive strength (UCS), theory predicts wall rock failure in positions opposite the direction of minimum far field stress and the wall rock will fail locally. In tunnels, fracture initiation often occurs significantly below the UCS with a familiar ratio of maximum tangential stress σ_θ/UCS of 0.4 ± 0.1, i.e. crack initiation beginning at ~ 0.4UCS. Whether wall fracture damage is by breakouts of intersecting shears or by tensile spalling due to radial extensional strain splitting (Stacey 1981; Martin et al., 1999; Shen 2008), theory allows calculation of σ_θ/UCS for circular openings. The Kirsch solution is scale independent and thus valid for cylindrical jetted holes typically of ~ 0.020 - 0.030 m in rotating nozzles, as well as tunnels e.g. >3m diameter. Note that in the case for tunnels, for initiation of wall failure, intact rock UCS may be replaced by a 'rock mass equivalent' Hoek-Brown strength criterion

based on for example a GSI rating with discontinuity strength reduction at the larger scale, giving an equivalent UCS. For brittle-elastic rock properties in RJD holes, whether servicing a producer or an injector mother-bore well, the pressure in the jet hole in this work is assumed to be approximately equal to the background formation pressure such that pore fluid pressures are equilibrated as in drained conditions and an in-situ effective stress analysis of failure is applicable. The conditions for initiation of instability for any overburden depth and k_H ratio (= σ_H/σ_v) or k_h ratio (= σ_h/σ_v) depending on whether the hole is parallel to minimum or maximum horizontal stress respectively can be simply estimated from a 2D analysis once the threshold value of σ_θ/UCS is set, e.g. at 1.0 or 0.4. The extent of breakout damage as a function of σ_θ/UCS is typically presented in terms of (i) breakout angle θ subtended at the vertical borehole centre and (ii) by damage radius r divided by hole radius R. Zoback et al., (1985), Shen (2008) and Kim et al., (2017) discuss breakout angles and depths of breakouts in the context of in-situ stress measurement in a borehole, based on 2D analytical theory and numerical models that consider the failure stress extending into the rock. For horizontal tunnels, a focus on the depth of a Highly Damage Zone and the deeper limit of Excavation Damaged Zone expressed by r/R, for σ_θ/UCS exceeding 0.4 was illustrated by Martin et al., (1999) with data for spalling initiation observed in various underground research laboratory (URL) sites and discussed recently by Perras and Diederichs (2016), see Fig. 3. Tunnel failure mechanisms resulting from tangential splitting and spalling are not necessarily prevalent in the smaller scenarios relevant to jet holes of ~ 35 mm diameter.

The objective of this paper is to consider jet-hole stability and breakage modes behind the jetting front as a function of rock deformability, strength and in-situ stress state. The methods used are 2D analytical elastic theory, FEM and a numerical simulation of progressive deformation using FEMDEM with a fracture model. For a recent summary of the principles behind the Solidity FEMDEM code, see for example Lei et al., (2017) where excavation damage and new fracturing beyond tunnel walls is modelled in rock masses with different intensity of pre-existing fractures. The analyses to be described below benefit greatly from observations of classical breakout behaviour seen in a new set of experimentally jetted holes performed at DTU (Fig. 5).

2. DEPTH, IN-SITU STRESS AND ROCK TYPE

To provide general guidance for stability and likely enlargement of holes due to breakouts, the Kirsch solution for circular holes is a good starting point. In the application below designed to simulate the TUD laboratory experimental jetting conditions, formation pressures are negligible. For in-service geothermal reservoir conditions at any depth, the pore fluid pressure in the formation may not follow an open hole hydrostatic gradient such as $\lambda = P_w/\sigma_v = 0.4$ and an effective stress

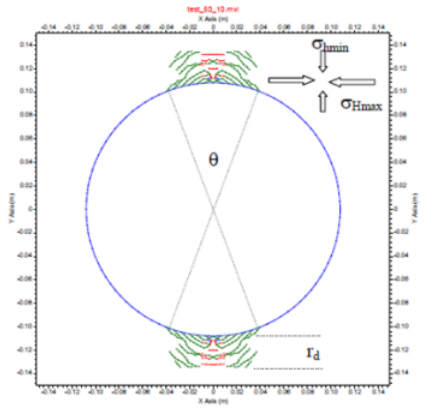

$$\frac{1-(\sigma_{H\max}+\sigma_{h\min})/\sigma_c}{2(\sigma_{H\max}-\sigma_{h\min})/\sigma_c}=\cos(\theta)$$

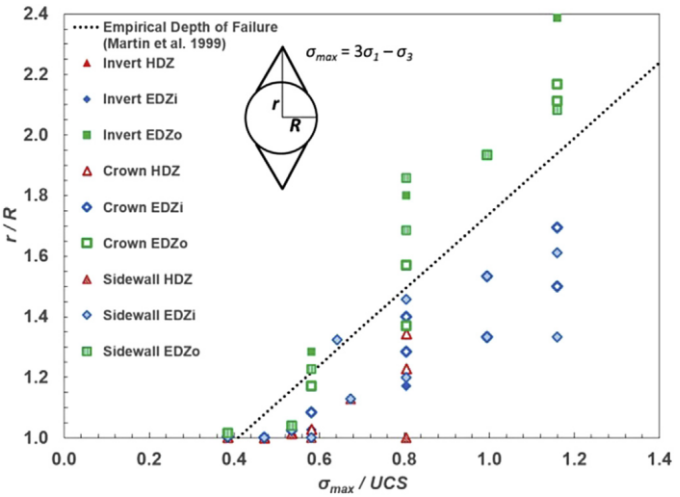

Figure 3. Theory for extent of breakout failures and damage zones Top: Shen (2008) Boundary element modelling of fractures using code FRACOD to obtain fracture style, location (giving angle theta) and depth into wall rock r_d of breakouts for case with σ_{Hmax} = 50 MPa, σ_{hmin} = 10 MPa. Middle: equation derivable from Kirsch solution for circumferential segment with tangential stress falling within range exceeding uniaxial strength σ_c. Bottom: Tunnel wall rock damage from Martin et al., (1999) showing Excavation Damage Zones and Highly Damaged Zone associated with breakouts, starting at σ_θ/UCS = 0.4, when the start of longitudinal splitting can occur.

analysis may require that raised pressures with e.g. λ = 0.6 be taken into account. Fig. 4 is calculated for λ =0.4. When the ratio σ_θ/UCS of maximum effective tangential stress to uniaxial compressive strength is increasing and found to exceed unity, e.g. as depth increases, or ratio k_H (= σ_H/σ_v) increases, or λ (= P_w/σ_v) increases or the rock strength decreases, then assuming the rock is 'jettable' in the first place, this threshold condition signals the end of relatively rounded (near to nozzle diameter) jet-holes. It

is relatively straight forward to construct a series of guide plots such as in Fig. 4. Consider the $k_H = 1.25$ case with UCS = 50 MPa, depths less than 1.0 km will have no breakouts. However, this threshold would drop to just under 0.5 km depth if the stress ratio $k_H = 2.0$. It is now interesting to speculate whether there is a suitable higher cut-off, e.g. say, when breakout behavior would be so advanced and acute that jetting equipment has operational problems with large fragment collapse behaviour occurring. The potential benefits of somewhat or significantly enlarged holes due to collapse may turn to disadvantages as σ_θ/UCS increases and exceeds a certain value, e.g. 3 or 4 perhaps?

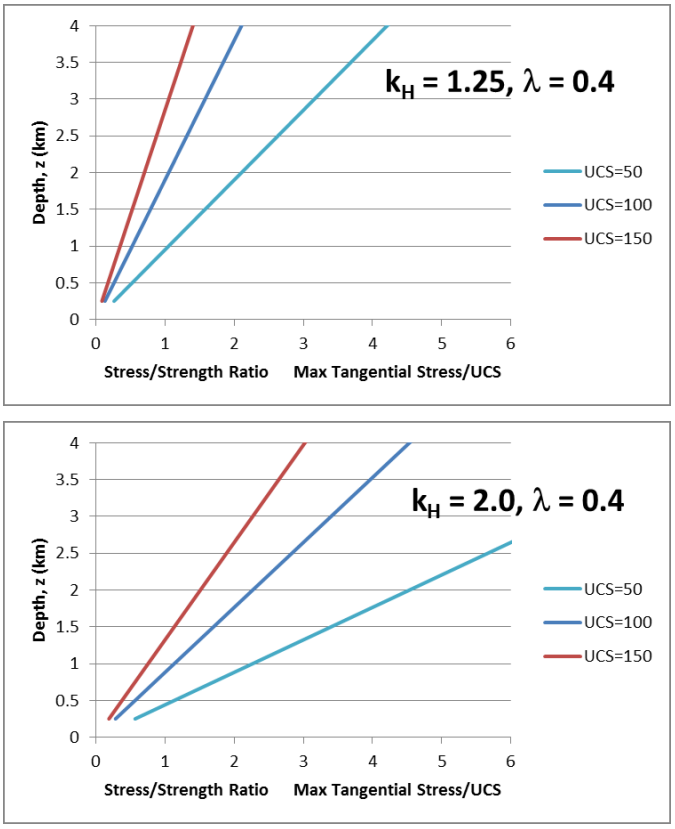

Figure 4. Example of construction of look-up plots for guidance on RJD lateral stability and regime of possible hole enlargement. (Hole parallel to σ_{hmin} strike-slip or thrust regime)

3. RESULTS

Jet drilling experiments with an 18 mm rotating nozzle were performed in TUD laboratories on 300 mm cubes of Gildehaus Sandstone under several states of true triaxial boundary conditions designed to investigate factors affecting rates of penetration. The apparatus can apply a maximum load of 3500 kN in each orthogonal direction (38.9 MPa with 300x300mm). Strain is calculated from displacement measurements (LVDTs) placed parallel to the loading directions. Jetting initiated at the centre of one of the cube-faces where a metal nut was glued into the rock, such that a feed-trough pipe could be mounted. This pipe also enabled the capture of outflowing water and debris for further analysis. Pore pressure in the rock could not be maintained due to edge effects (pistons should not touch each other). It is therefore assumed that the pore pressure is nearly atmospheric throughout testing, except locally where the jets impinge. The geometry of the excavated holes were determined using a (medical grade) X-ray CT scanner as installed at the TU Delft GSE laboratory, and subsequent 3D image processing using commercially available dedicated software (Avizo. Thermo Fisher). We assume that the geometric form represents the equilibrium state of each hole at the moment drilling action was terminated prior to unloading the test rig applied stresses (Fig. 5), and no further inelastic deformation was caused by unloading the samples. Geometric variations of the resulting jetted advancing front and side wall can be compared for example with an idealised smooth wall 18 mm cylindrical hole. The stress fields for idealized circular and actual profiles were then examined using FEM to predict the state of stress as a proportion of failure stress, based on known boundary in-situ stresses together with strength and deformability properties of Gildehaus Sandstone (Table 2).

Table 1 TUD True triaxial test conditions across the hole giving tangential stress/UCS strength ratio according to the Kirsch solution and assuming Gildehaus Sst UCS of 53 MPa.

Test Jetting	$\sigma_\theta = 3\sigma_{max} - \sigma_{min}$ MPa	σ_θ/UCS	σ_{max} MPa	σ_{min} MPa
J03	10	0.189	5	5
J04	80	1.509	30	10
J02	100	1.887	35	5

Table 2. Material properties of Gildehaus Sandstone applied to FEMDEM simulation

Material Property	Gildehaus Sst
Young's modulus E GPa	19.5
Poisson's ratio v	0.265
Bulk Density (kg/m^3)	2000
Tensile strength MPa	3.5
Internal friction angle degrees	23
Cohesion MPa	17.6
UCS MPa	53
GIc J/m^2	100
GIIc J/m^2	1750

Experiments were also performed to explore the effects of stress magnitude and orientation on the overall jetting performance (i.e. rate of penetration) as well as jetting into fractures / voids to study potential curving effects. However, we restrict reporting to consideration of an assumed 2D stress field independent of stress in the hole axis (y) direction. Moreover, regardless of the stress

conditions of each experiment, the resulting jetted borehole was straight. Variations along the borehole axis are only evident at the furthest leading edge, where the back-thrusters (see Fig. 1) have not reached. Here, at the borehole tip, the borehole is generally circular and narrower. Fig. 5 shows the distinctive jet-hole responses.

To explore effects of far field stress prior to excavation by jetting and the potential for wall-rock failure, methods used in this paper first consider application of FEM to idealized circular holes and then the actual profiles. Simulating the same conditions as the experimental set up, a 300 mm edge cube was created with the CAD software Rhinoceros. Different hole shapes have then been subtracted from the cubic volume. The resulting geometries were then imported into MATLAB and the effects of the applied triaxial stresses could also be simulated with the 3D FEM PDE solver in MATLAB. Here we have applied the in-situ stresses just in the 2D plane-strain model: σ_v on the top edge, σ_h on the left edge and roller constraints on the right and bottom edges.

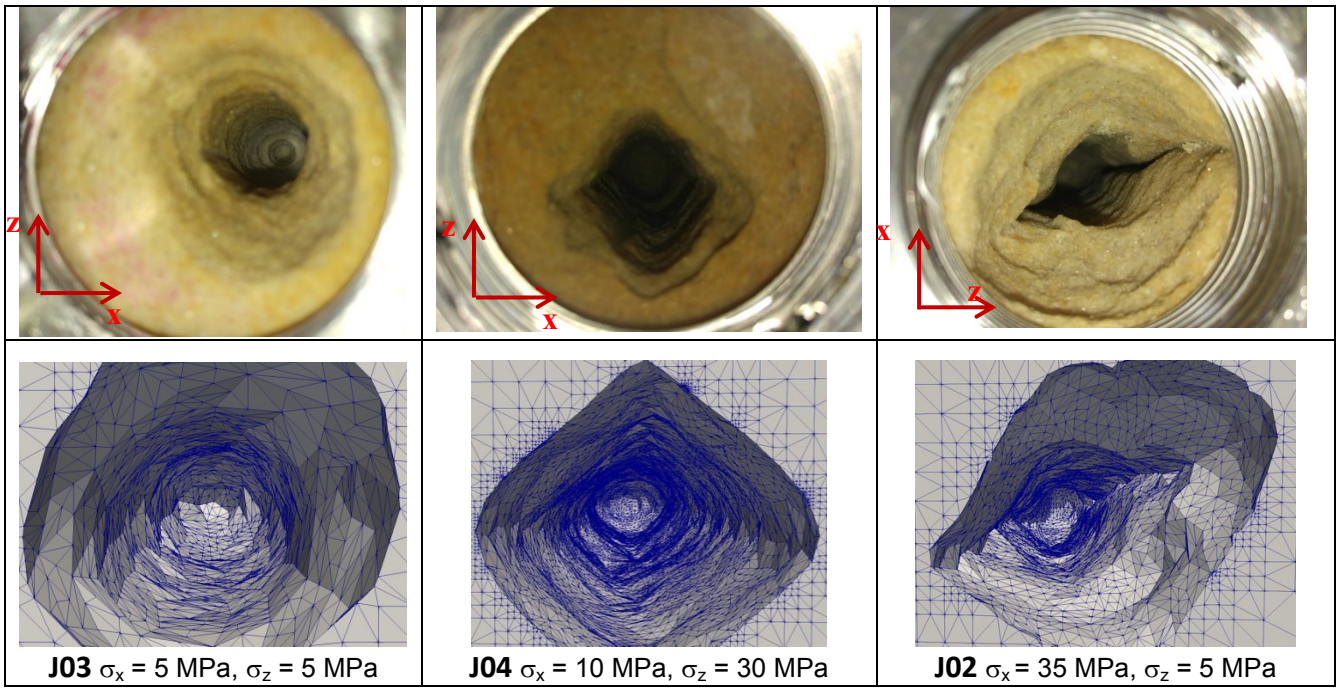

Figure 5. Top: Wall rock breakdown responses to Rotating Nozzle Jet Drilling in True Triaxial stress conditions (from results of TUD tests). Metal threaded access diameter is ~ 60 mm, giving circular view of sandstone and jet hole. Bottom: X-Ray CT scan details of hole geometry visualized down hole including 3D surface mesh in preparation for future work on 3D stress analysis.

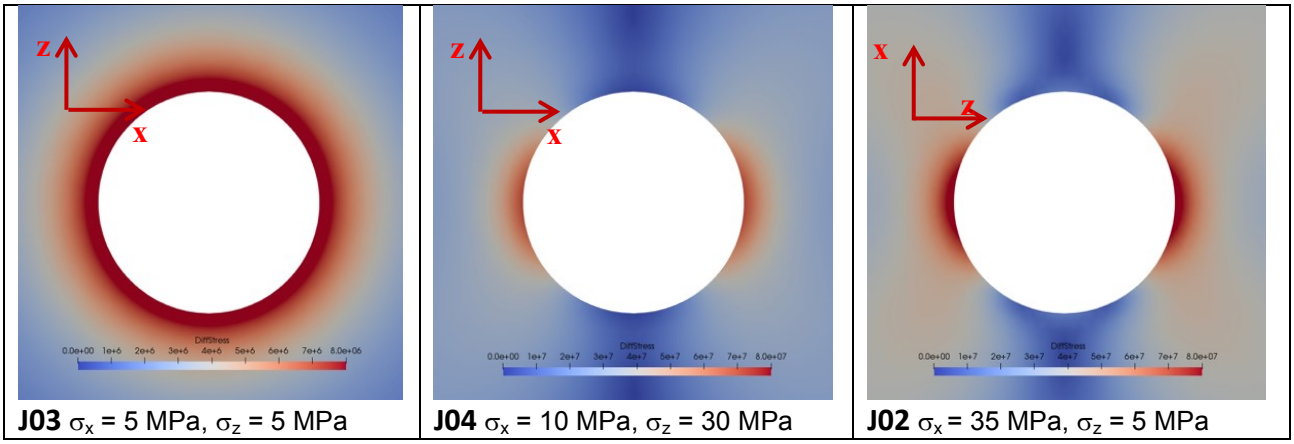

Figure 6. Idealised circular hole FEM stress solutions considering stress states for three triaxial jetting tests shown in Fig.5. Results confirm Kirsch solutions. For J03, the differential stress scale is an order of magnitude lower where the tangential stress is uniformly 10 MPa (Table 1).

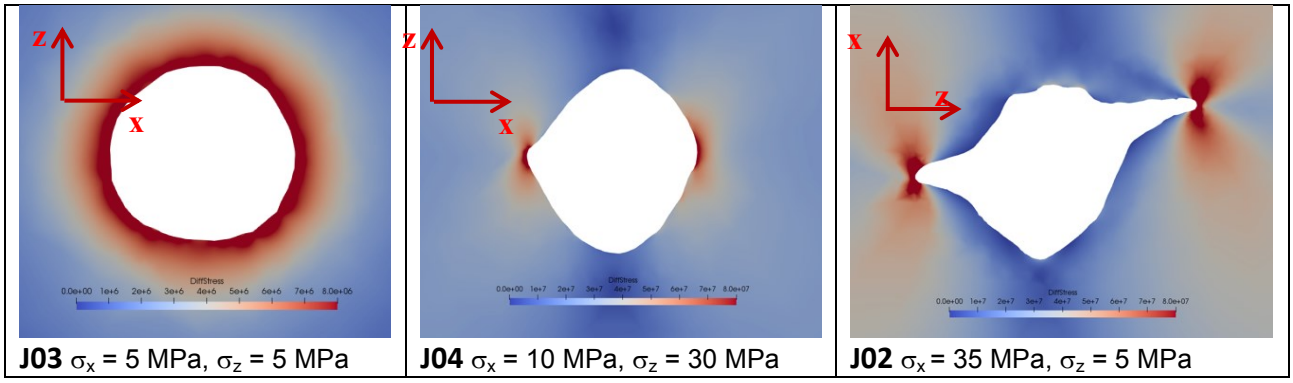

Figure 7. FEM 2D plane strain analysis for sampled cross sections of actual jetted holes, considering stress states for three triaxial jetting tests shown in Fig.4. J03 is near to cylindrical so the result is similar to te one as shown in Fig.6.

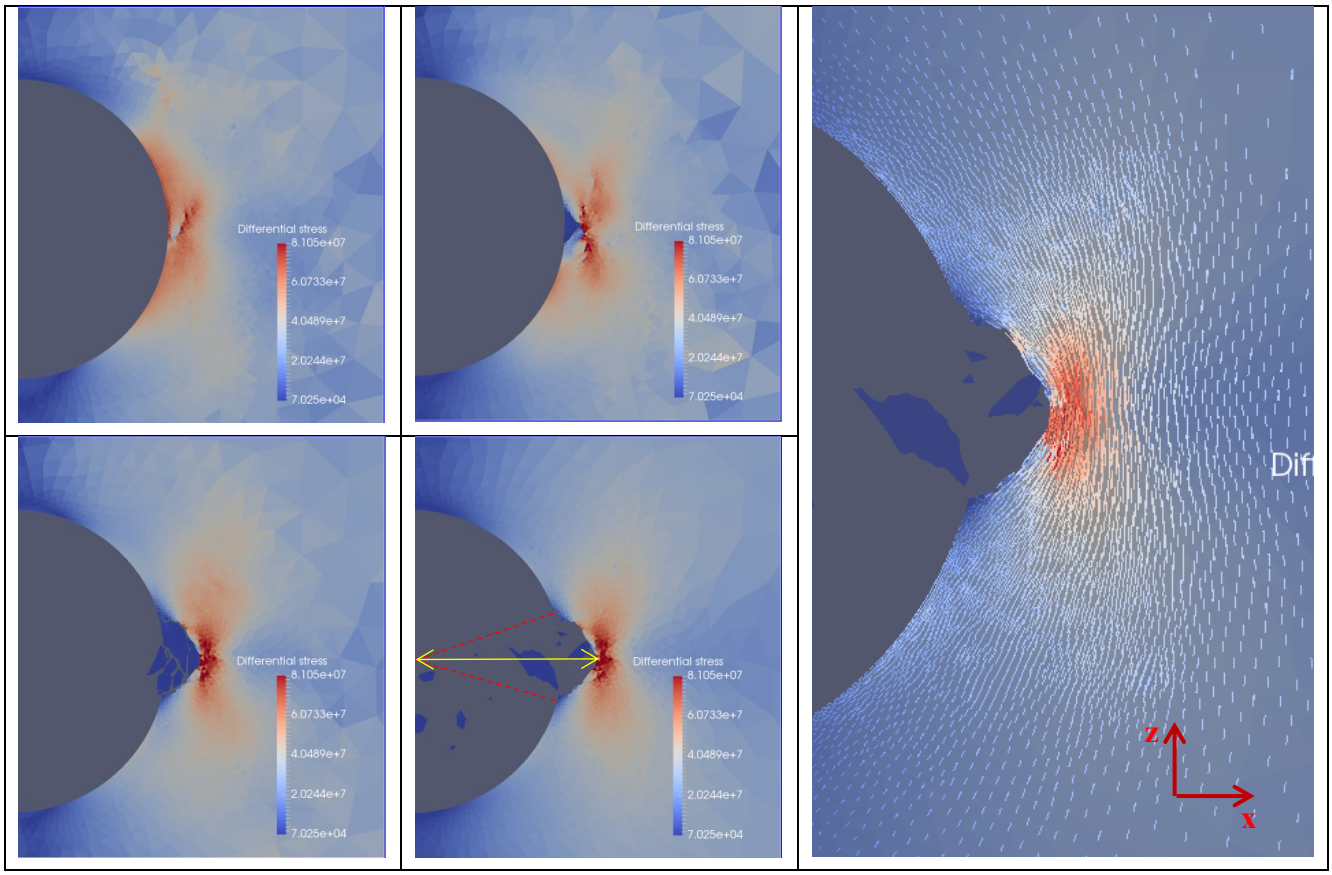

Figure 8. Details from 2D FEMDEM Simulation with Solidity code, representative of J04 biaxial conditions with σ_x = 10 MPa, σ_z = 30 MPa. Top left: Initiation of shear failure; top right: symmetric breakout formed with unloaded wedge; bottom left: enlargement of breakout zone, deepening and widening, with fragmentation and removal; bottom right: furthest extent of breakout, equilibrium reached; far right: σ_1 stress trajectories refracted showing maximum advance of failed breakout zone.

3.1 FEM analysis of stress for a circular hole

The FEM analysis in Fig. 6 simply reproduces the analytical Kirsch solutions as the 300 mm sides where the boundary stress is applied is far away from the hole.

3.2 FEM analysis of stress for a final 2D section of observed hole

Looking down J04 and J02 in Fig. 5, there is quite a lot of variability in geometry. Nozzle vibration may be influencing the profiles in J04 seemingly helping to broaden the hole top and bottom while the breakout corner is apparent on the left. As the hole walls were in equilibrium but in a critical state reflecting the extent of breakouts when testing ended and unloading began, the FEM differential stress on unconfined walls near expected breakout zones are somewhat higher (~80 MPa) that the large specimen laboratory tested UCS value of 53 MPa. For the J02 case with exceptional and unrealistically high stress ratio of 7:1, the extreme breakout looks like the dog-ears may be transitioning

into compaction bands or else the tip extension is enhanced by jet flow erosive action. Very locally in the tips, the differential stress computed from FEM appears high enough to fail this rock in compression by shear. This 2D analysis may be over representing the actual maximum differential stress experienced in the 3D experiment.

3.3 FEMDEM analysis - circular holes

The true loading history in the laboratory test is one of disturbing a far field equilibrium state by excavation unloading and dramatically increasing tangential compressive stresses in the excavation wall rock. The 2D stress field for a cylindrical opening some two diameters behind the jetting front evolves from far field to fully developed Kirsch solution values. The FEMDEM simulation was performed by an alternative loading history to that in the actual complex jet drilling tests. In each of the three simulations, an unstressed block with a central hole already existing is subjected to gradually and linearly increasing loading from zero up to the laboratory experimental biaxial stress values given in Fig. 5 and maintaining the far-field stress ratio during the stress ramping phase. Thereafter the boundary stresses are held constant.

For J03, with a stress ratio of 1 (5 MPa, 5 MPa), the maximum stress values of about 10 MPa in the FEMDEM model bear out the FEM predictions of Fig. 6 and a uniform hoop stress is seen.

For J04, with a stress ratio of 3 (30 MPa, 10 MPa), failure is initiated almost exactly when the stress reaches the top of the ramping phase with differential stresses peaking at around 81 MPa. It is noted that in Fig. 8 bottom right, the observed breakout angle of 36^0 is small compared with the theoretical value of 75^0 from classical theory (see equation in Fig. 3) and the ratio r/R of 1.22 appears quite compatible with the ~36^0 breakout angle. The empirically observed tunnel breakout depth value for r/R of 1.22 is when σ_θ/UCS = 0.6

For J02, with a stress ratio of 7 (35 MPa, 5 MPa), this is a very extreme case. We anticipate from the Kirsch solution (Figs. 2 and 3) a well-developed tensile failure occurring in the x-direction $\sigma_{\theta min}$ = -20 MPa (well in excess of Tensile strength (3.5 MPa) while breakouts by shear failure would occur opposite z with $\sigma_{\theta max}$ = 100 MPa. For this case, results shown in Fig. 9 appeared only partially capable of charting the progressive development of the hole profile, results becoming numerically unstable prior to the full ramp stage being achieved owing to the initial mesh refinement being inadequate at a certain distance from the hole. However, the tensile fractures can just be seen. The breakout pattern reverts to sharp cusps as actually seen in J02 near the jet entrance to the block (Fig. 5). This is reminiscent of compaction bands. Furthermore, the jetted lateral's evolved shape may be influenced by the erosive forces of the water jet flows enlarging the excavated breakout features.

In all three cases considered, for practical operations in the laboratory (and in the field) the jet nozzle and coil tubing will vibrate and create holes significantly larger than the nozzle diameter, as observed in J03 even under benign isotropic stress and low confinement i.e. easy drilling conditions. The right angle simulated breakouts of the J04 simulation are compatible with the laboratory test jet holes seen in J04 with almost right-angle corners if we assume the nozzle vibration has contributed to a more rounded enlargement in the z direction.

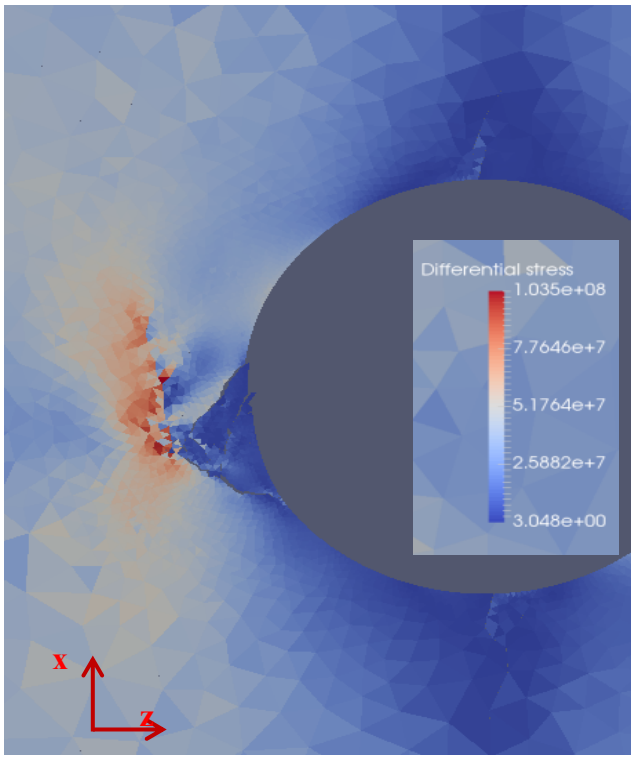

Figure 9. 2D FEMDEM Simulation, representative of J02 biaxial conditions with σ_x = 35 MPa, σ_z = 5 MPa. Note evidence of tensile fractures opposite x.

3.4 Complex shape profiles

Preliminary simulations for a few complex shape sections were performed with the FEMDEM code subject to a ramping stress rising to 30:10 MPa. The simulation (Fig. 10) indicates a wall rock bearing a maximum differential stress of 53 MPa (i.e. UCS) in the jetted hole excavated in Gildehaus sandstone. This reassuring result from a modelling view point indicates that all the fracturing and or hole enlarging mechanisms that would have occurred in the original jetting tests have been completed, such that the hole under service conditions would be mainly stable and possibly quasi-stable at two extreme locations opposite the minimum

far field stress, with no threat to the serviceability of the hole.

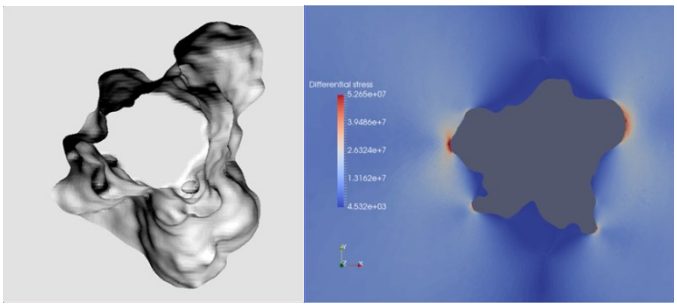

Figure 10. Visualisation from X-Ray CT and FEMDEM stress analysis of this profile showing no further fracturing is expected.

4. CONCLUDING REMARKS

This research has raised the interesting possibility that an initially jetted hole may become enlarged through breakout instabilities. Under progressive deformation, these can be expected to eventually stabilise as far field maximum principal stresses refract around the hole. If the fragmentation by breakouts is occurring while sufficient energy from the jetting fluids is capable of comminuting and clearing the largest rock fragments, taking them away in suspended fluids in the return flow annulus, then to some extent breakout behaviour could be beneficial to enhancing heat exchange and higher rates of hot fluid flows. Further research is required to investigate theoretical and practical limits to the existence of such a potential benefit. Future laboratory tests could include anisotropic rocks and the effects of pore pressure if the sample can be properly sealed. Further numerical simulation using FEMDEM tools informed by 3D stress fields behind a jetted front and more realistically phased loading histories are planned for future work. Such studies may help provide an understanding of when the stress to strength ratio is simply too high for practical operations.

ACKNOWLEDGEMENTS

This project has received funding from the European Union's Horizon 2020 research and innovation programme under grant agreement No. 654662. RB would like to thank the TU Delft Geoscience and Engineering laboratory staff for technical and imaging support.

REFERENCES

Brehme, M., S. Regenspurg, P. Leary, F. Bulut, H. Milsch, S. Petrauskas, ... & G. Blöcher. 2018. Injection-Triggered Occlusion of Flow Pathways in Geothermal Operations. *Geofluids*, Article ID 4694829, 14 pages.

Eberhard E. 2001. Numerical modelling of three-dimension stress rotation ahead of an advancing tunnel face. *International Journal of Rock Mechanics & Mining Sciences* 38: 499–518.

Kim, H., Xie, L., Min, K-B. Bae, S. and Stephansson, O. (2017) Integrated In Situ Stress Estimation by Hydraulic Fracturing, Borehole Observations and Numerical Analysis at the EXP-1 Borehole in Pohang, Korea *Rock Mech Rock Eng* 50: 3141.

Kirsch, C. 1898. Die theorie der elastizitat und die bedurfnisse der festigkeitslehre. *Zeitschrift des Vereines Deutscher Ingenieure*, 42:797{807}.

Lei, Q., Latham J-P., Xiang, J., Tsang, C-F. 2017. Role of natural fractures in damage evolution around tunnel excavation in fractured rocks, *Engineering Geology,* 231:100-113.

Martin, C.D., Kaiser, P.K. & McCreath, D.R. 1998. Hoek–Brown parameters for predicting the depth of brittle failure around tunnels. Can. Geotech. J. 36:136-151.

Perras, M. A., and Diederichs, M. (2016) Predicting excavation damage zone depths in brittle rocks. *Journal of Rock Mechanics and Geotechnical Engineering* 8: 60-74.

Shen, B. 2008. Borehole breakouts and in-situ stresses SHIRMS 2008, eds. Y. Potvin, J. Carter, A. Dyskin, R. Jeffrey. Australian Centre for Geomechanics, Perth.

Stacey, T.R. 1981. A simple Extension Strain Criterion for Fracture of Brittle Rock. *Int. J. Rock Mech. Min. Sci. & Geomech. Abstr.:* 18, 469-474.

Zoback, M.D., Mooss, D., Mastin, L. and Anderson, R. (1985) Wellbore breakout and in situ stress, *Journal of Geophysical Research*: 90(B7), 5523–5530.